Iranian Journal of Medical Physics

ijmp.mums.ac.ir

Evaluation and Comparison of Iodine-Based and Biosynthesized Gold Nanoparticles as X-Ray Contrast Agent and Their Effects on Renal Functions in Male Wistar Rats

Paul Sola Ayanlola[1], Gbadebo Adebisi Isola[1], Waidi Adeoye Saka[2,*], Margaret Kofoworola Akinloye[1], Abraham Adewale Aremu[1], Mustapha Kola Lawal[3]

1. Department of Pure and Applied Physics, Faculty of Pure and Applied Sciences, Ladoke Akintola University of Technology, Ogbomoso, Oyo State, Nigeria.
2. Department of Physiology, Faculty of Basic Medical Sciences, Ladoke Akintola University of Technology, Ogbomoso, Oyo State, Nigeria.
3. Department of Science Laboratory Technology, Faculty of Pure and Applied Sciences, Ladoke Akintola University of Technology, Ogbomoso, Nigeria.

ARTICLE INFO

Article type:
Original Paper

Article history:
Received: Aug 03, 2023
Accepted: Feb 19, 2024

Keywords:
X-Ray Contrast Agents
Iodine-Based
Biosynthesized
Nanoparticles
Gold Nanoparticles
Renal Functions

ABSTRACT

Introduction: Gold nanoparticles (AuNPs) have gained significant attention as a promising contrast agent to overcome the challenges of iodine-based contrast agents (ICAs), such as poor contrast, and renal toxicity. However, studies have associated toxicity with AuNPs synthesized through chemical methods, thereby raising concerns regarding the safety of such AuNPs. This study, hereby, compares the performance of iodine-based and biosynthesized AuNPs from the extract of *Psidium guajava* and *Corchorus olitorius* as CA on radiographs and renal functions of rats.

Material and Methods: 156 rats were grouped into baseline (A), experimental control (B), ICA (C), and two AuNPs groups (D and E). The ICA (Urografin 76%), AuNPs, 8.23±1.03 nm (from P. guajava), and 6.57±1.62 nm (from C. olitorius) were administered to the rats in groups C, D, and E respectively. The rats, excluding group A, were radiographed, and samples of blood and kidney tissue were collected on days 1 and 30 for the assessment of renal functions.

Results: The rats injected with the AuNPs showed radiographic contrast with anatomical features better than those without CA and those injected with the ICA. The biochemicals showed a significant decrease in renal functions for the rats injected with the ICA while those injected with the AuNPs protected against nephropathy when compared with those without CA and those injected with ICA.

Conclusion: It was revealed that biosynthesized AuNPs can be a suitable replacement for the ICA because of the high atomic number and attenuation properties of gold, the increased surface area of AuNPs, and biocompatibility.

►*Please cite this article as:*
Ayanlola PS, Isola GA, Saka WA, Akinloye MK, Aremu AA, Lawal MK. Evaluation and Comparison of Iodine-Based and Biosynthesized Gold Nanoparticles as X-Ray Contrast Agent and Their Effects on Renal Functions in Male Wistar Rats. Iran J Med Phys 2024; 21: 295-305. 10.22038/ijmp.2024.74142.2316.

Introduction

The aim of radiography is to capture images of internal organs and tissues that are suitable for diagnostic and therapeutic purposes. However, some anatomical structures may closely resemble their surrounding tissues in physical properties, making them difficult to differentiate radiographically. To address this issue, contrast agents (CAs) are utilized in X-ray radiography to improve the technique's sensitivity, assist in identifying abnormalities in radiographic images, and produce high-resolution images [1]. Once administered, the distribution and circulation of the CA are influenced by the cardiovascular system. However, its distribution can impact and disrupt the hemodynamics of the system and other organs, such as the kidneys and liver, through which the substance passes [1, 2]. The x-ray CAs currently in use are primarily composed of iodine molecules (atomic number Z = 53) and often encounter challenges related to limited imaging time, potential renal toxicity, and inadequate contrast in larger patients [3,4]. Iodine-based contrast agents (ICAs) can be harmful to the kidneys and may trigger acute kidney injury (AKI) or worsen existing chronic kidney disease (CKD). It has been observed that AKI caused by iodine-based contrast agents is the third leading cause of acute renal failure in hospitalized patients, following renal hypoperfusion and medications [5], accounting for 11% of AKI cases [6, 7]. Despite its clinical significance, the growing use of contrast agents in radiological procedures has led to a rise in the occurrence of

*Corresponding Author: Tel: +2348063101718; Email: wsaka@lautech.edu.ng

contrast-induced nephropathy [8]. Contrast-induced nephropathy (CIN) refers to the iatrogenic decline in kidney function after the use of contrast agents in the absence of other nephrotoxic substances [9]. This condition is the result of a combination of hypoxic and toxic damage to the renal tissue, influenced by reactive oxygen species [10].

Reactive oxygen species (ROS) are oxygen-containing molecules that are chemically reactive and serve multiple beneficial functions in living organisms. These molecules are essential for various physiological processes, including intracellular signaling, maintaining homeostasis, regulating cell death, defending against pathogens, and triggering mitogenic responses [11 - 15]. ROS are typical by-products generated during normal aerobic cellular metabolism of oxygen and can also be produced by external factors like ultraviolet light, ionizing radiation, lifestyle choices, diet, stress, smoking, and other foreign substances. To effectively manage the levels of free radicals and sustain a balance between reducing and oxidizing states, living organisms have antioxidant defense mechanisms in place [16 – 21]. However, oxidative stress (OS) arises when there is a discrepancy between the generation of reactive oxygen species (ROS) and the ability of antioxidant systems to neutralize these reactive substances. An overabundance of free radicals produced in OS conditions leads to oxidative harm to proteins, lipids, and nucleic acids, thereby jeopardizing cell health and aiding in the progression of diseases [22, 23]. Research indicates that administering CA boosts ROS production and renal oxidative stress, leading to damage to cell membranes, either directly [24] or indirectly [25]. Additionally, it has been reported that CA administration reduces oxygen levels in medullary structures of the kidney without affecting tubular reabsorption [26].

Scientists have suggested using nanoparticles (NPs) as contrast agents (CAs) in X-ray imaging to address the kidney toxicity linked to iodine-based CAs [27 – 29]. Among metals with higher atomic numbers (Z) than iodine (Z = 53), gold-incorporated nanoparticles (AuNPs) have attracted attention as a promising CA due to their plasmonic properties, low toxicity compared to other metal-based NPs, excellent colloidal stability, easy manipulation, nontoxicity, and simple synthesis [27, 29 - 32]. Additionally, gold possesses a high atomic number (Z = 79) and exhibits a greater attenuation coefficient at diagnostic energy levels compared to iodine, allowing it to absorb more X-rays at certain energy levels [33]. Numerous techniques for synthesizing AuNPs have been reported in the literature, focusing on controlling size, morphology, and surface chemistry, with the majority relying on physical or chemical methods that tend to be costly and lack biocompatibility [34, 35]. Research has linked exposure to AuNPs produced from these two methods with toxicity, noting heightened ROS generation, mitochondrial harm, inflammation, DNA damage, and even instances of apoptosis or necrosis [36, 37]. These studies also highlight concerns about the impact of AuNPs on other organs when utilized in various biomedical applications. Given the function of the proximal tubules and the kidneys' significant role in excretion, this organ is particularly vulnerable to the impact of xenobiotics [38, 39]. The interaction between AuNPs and the kidneys naturally occurs in vivo because of their distribution and elimination in the renal system. Consequently, as there is an interest in employing AuNPs as radiocontrast, it is essential to develop novel AuNPs that are non-toxic and biocompatible through biological methods.

The utilization of the biological approach involves either plants or microorganisms, with plants and their materials offering certain advantages over microorganisms [34, 35]. Plants and associated materials are preferred for synthesizing NPs because it eliminates the need to maintain microorganisms, streamline the process without multi-step procedures [40, 41], and enable easy scaling up for large-scale production [42]. This research leveraged the bioavailability and phytochemical properties found in *Psidium guajava* (guava) and *Corchorus olitorius* (Jute mallow) plants, both of which have demonstrated medicinal benefits [43 - 45]. Furthermore, it has been reported that AuNPs derived from these two plants safeguard the cardiac cells and improve cardiac function [2]. Therefore, this study examines and compares the effectiveness of iodine-based radiocontrast and plant-based AuNPs as contrast agents in radiography while also evaluating their impact on renal function, given that X-ray imaging can be used at any stage of life and with different tube voltages. This will also support the use of biosynthesized AuNPs as contrast agents and alleviate concerns about the cellular toxicity of chemically synthesized AuNPs in biomedical applications.

Materials and Methods

Biosynthesized gold nanoparticles

The AuNPs utilized in this research were produced from *P. guajava* and *C. olitorius* plants, with a concentration of 1 mM chloroauric acid ($HAuCl_4$ prepared from gold (III) chloride hydrochloric acid ($HAuCl_4.3H_2O$), Sigma-Aldrich and used without further modification). The method followed in this study was based on a previous investigation [2]. In summary, 1 mL (*P. guajava*) and 3 mL (*C. olitorius*), identified as optimal, were each combined with 20 mL 1 mM HAuCl4 and stirred for 10 minutes using a magnetic stirrer. The samples that were prepared underwent UV-Vis, x-ray diffraction, energy-dispersive X-ray, and transmission electron microscopy analysis to determine the absorbance spectroscopy, crystalline structure, elemental composition, and morphology of the synthesized samples, respectively. Table 1 summarizes the properties of the two biosynthesized AuNPs, while Figures 1 a and b reveal their nature.

Table 1. Summary of the nano-characteristics of the plant-based AuNPs

Parameters	*P. guajava*	*C. olitorius*
Plasmon resonance wavelength	534 nm	538 nm
X-ray diffraction pattern	(111), (200), (220)	(111), (200), (220), (311)
Elemental composition (Au % weight)	75.52%	74.74%
Particle size	5 – 11 nm	3 – 10 nm
Average diameter	8.23 ± 1.03 nm	6.57 ± 1.62 nm
Shape	Spherical	Spherical

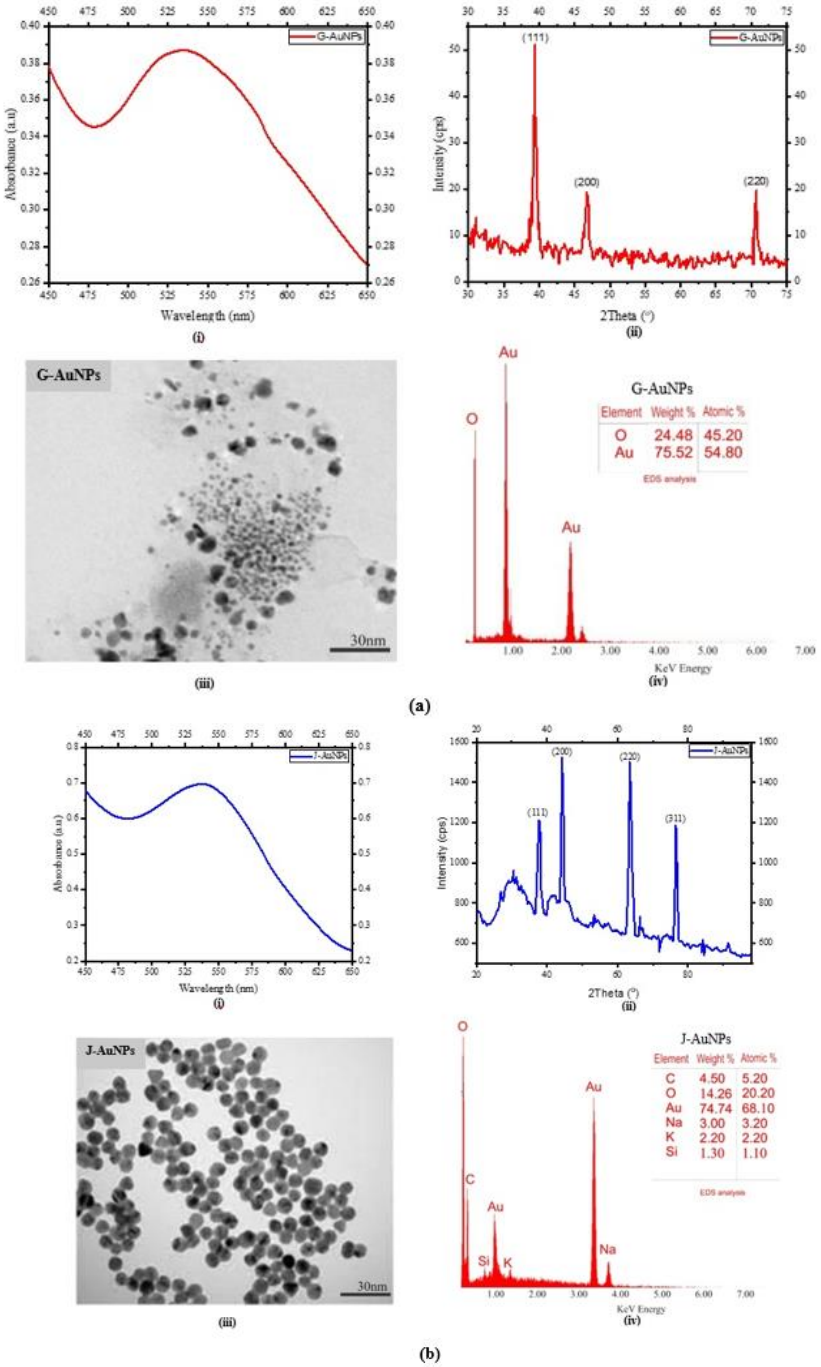

Figure 1. Characteristics properties of the plant-based AuNPs (a) *P. guajava (*guava) (b) *C. olitorius* (Jute mallow). The images revealed the (i) UV-Vis absorbance spectra, (ii) X-ray crystalline structure, (iii) morphology, and (iv) elemental composition of the biosynthesized AuNPs.

Experimental design and treatment

One hundred fifty-six male Wistar rats, averaging 100 ± 20 g in weight, were handled in accordance with global practices [46], with the protocol sanctioned by the Research Ethics Review Committee of the Ministry of Health in Oyo State, Nigeria, under reference number AD13/479/2070B. To ensure the study utilized healthy subjects, the rats were allowed a period of acclimatization during which their average body weight reached 270 ± 25 g. Food and water were withheld from the rats for 24 hours prior to the initiation of treatment.

Table 2. Experimental distribution and treatment of the rats

Control	Treated				
	Tube Voltage (kV)				
A		B	C	D	E
12	40	12	12	12	12
	80	12	12	12	12
	120	12	12	12	12

A: Baseline control/untreated, B: Experimental control/ no substances were administered but exposed to x-ray only; C: administered with the ICA (Urografin) and irradiated; D: administered with the P-AuNP and irradiated; E: administered with the C-AuNP and irradiated.

The rats were subsequently randomized into two groups: control (group A) and treatment (groups B, C, D, and E), as shown in Table 2. Rats in groups C, D, and E received intraperitoneal injections of ICA, P-AuNPs, and C-AuNPs at a rate of 6 mL/kg [47 - 49]. The rats in the treated groups were restrained and irradiated at 40, 80, and 120 kV of x-ray respectively, with an exposure current of 8 mAs at the distance from source to subject (rats) of 1 m using MARS Fixed X-ray, Allengers Medical Systems Ltd.

Sample collection and preparation

On days 1 and 30 of the experiment, six rats from each group/replicate of the control and exposure were sacrificed by cervical dislocation and cardiac punctures were used to obtain blood samples. Serum was thereafter extracted from the blood following standard laboratory procedure. The kidney was removed and split in half; a part was promptly preserved in 10% formal saline and preserved pending histopathological analysis. The other half was rinsed in regular saline, and 5 ml of the tissue was homogenized with 10 mM phosphate buffer on ice. The supernatant was then obtained by centrifuging the mixture for 5 minutes at 10,000 rpm. While awaiting biochemical analysis, the tissue supernatant and serum were kept at -80°C.

Evaluation of biochemicals

The tissue homogenate and serum samples were withdrawn, and an aliquot of the sample was examined for the presence of oxidative stress markers, including blood urea nitrogen (BUN), creatinine (CRE), sodium (Na), potassium (K), calcium (Ca), bicarbonate (HCO_3), glutathione (GSH), malondialdehyde (MDA), and catalase (CAT). By employing colorimetric techniques with suitable commercially available reagents and adhering to the manufacturer's instructions, the activity level of each parameter was ascertained.

Histopathology evaluation

The fixed kidney specimens were retracted and ready for histological analysis following standard laboratory protocol. The serial sections were suitably stained, and any anomalies in the tissue morphology were observed under a light microscope

Data analysis

The values obtained for each biochemical parameter investigated were treated statistically using ANOVA and Dunnett's post-hoc test at 0.5 levels of significance with GraphPad Prism (9.1.0 (221). The data were presented as mean ± standard error of the mean (SEM). The grayscale of the obtained radiographs was subsequently quantified using ImageJ software (1.53e, National Institutes of Health, USA).

Results

Contribution of each substance to radiographic contrast

Figure 2 shows the radiograph and characteristics of the rats exposed at 40, 80, and 120 kV without any of the substances, and Figure 3 shows the radiograph of rats in the experimental control group, those injected with ICA, and the biosynthesized AuNPs, respectively. The area with high density (low brightness) indicates an area where the X-ray beam has been transmitted, while the area with low density (high brightness) indicates an area where the X-ray beam was absorbed by the rats. The observation of the radiograph in Figure 2a showed that there was no significant difference in the radiograph of the rats at each of the x-ray tube voltages, as revealed by the characteristics in Figure 2b. Thus, it can be inferred from the rat's radiograph that the higher the kV, the greater the penetrability of the beam through the rats and, hence, no significant contribution to the radiocontrast.

In Figure 3, the radiograph appeared blurred (no contrast) for the rats of the experimental control (without any of the substances, Figure 3a), while the rats injected with the iodine-based CA (Urografin) showed little contrast (Figure 3b) compared to those of Figure 3a. The implication of this is that to achieve sufficient contrast of the radiograph suitable for diagnostic interpretation, it is either the dosage of ICA or the kV of the x-ray machine is increased, both of which expose the rats unnecessarily, causing damage to the biological system. However, the rats injected with the biosynthesized AuNPs from the guava extract (Figure 3c) and Jute mallow (Figure 3d) revealed more distinguished anatomical parts (more contrast) in comparison to that of groups B (Figure 3a) and C (Figure 3b). The analysis of the radiograph (Figure 3e) showed a significant reduction in the intensity of the grayscale from 0 (black) to 255 (white), with the rats of groups D and E exhibiting better contrast (brightness), and this further corroborated the difference in the quality of the radiograph obtained for the imaged rats.

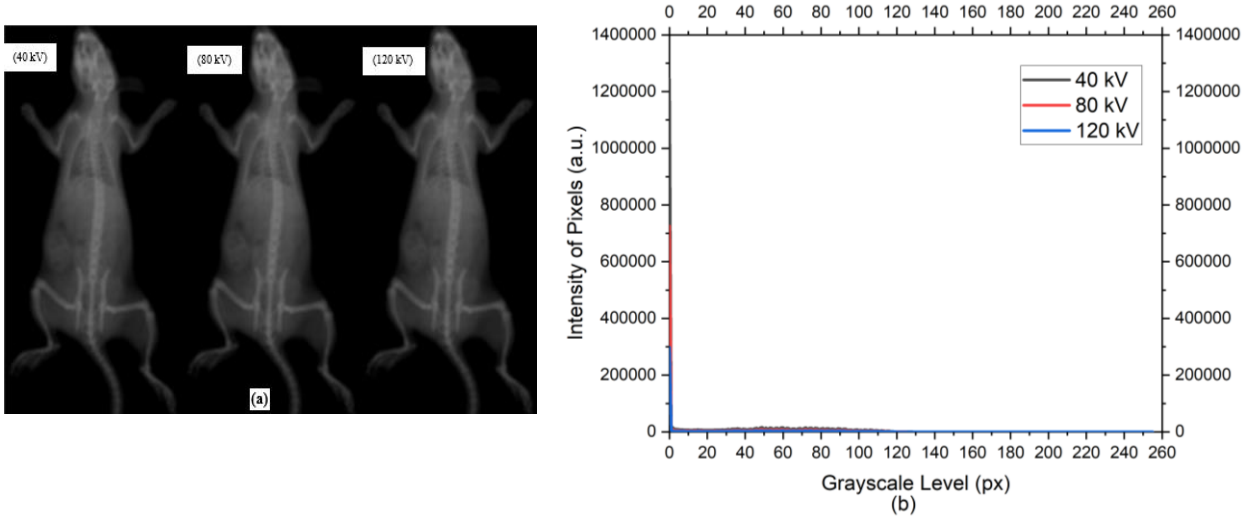

Figure 2. (a) Radiograph (b) difference in intensity of the grayscale of rats without any of the administered substances at 40, 80, and 120 kV respectively

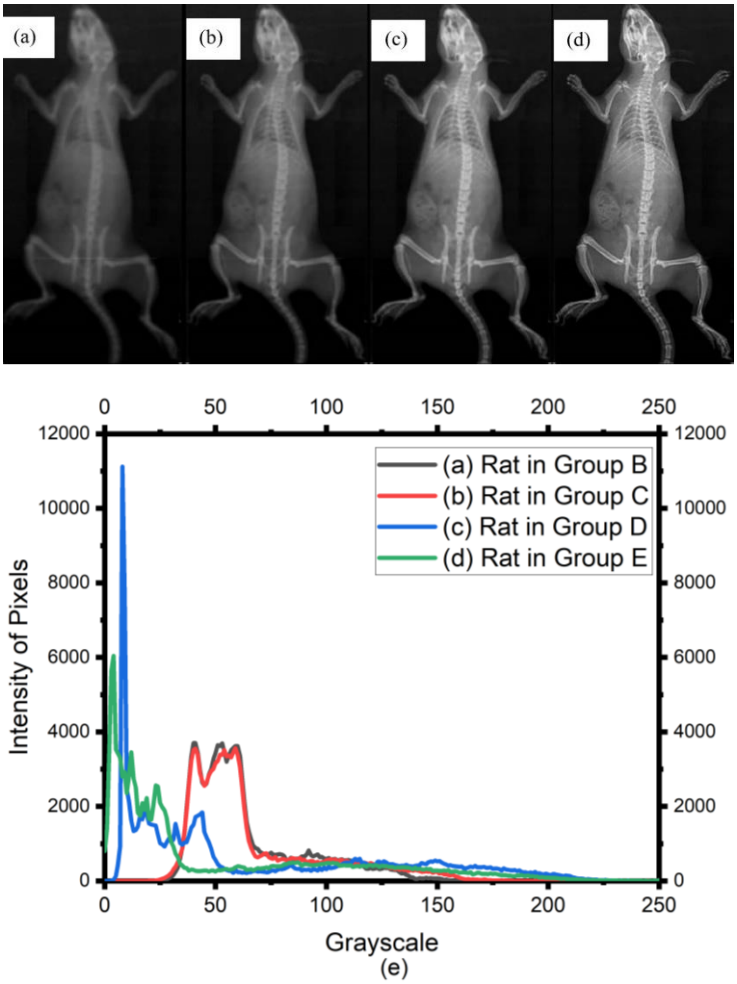

Figure 3. Radiograph of (a) group B rats, without CA (b) group C rats, injected with iodine-based CA, Urografin (c) group D rats, injected with *P. guajava* capped AuNPs (d) group E rats injected with *C. olitorius* capped AuNPs (e) difference in intensity of the grayscale of the imaged rats.

Table 3a. Kidney biochemical levels of the untreated and the treated rats at 40 kV on day 1.

Indicators	A	B	C	D	E
SOD (µmol/g tissue)	12.16 ± 0.83	9.27 ± 0.43	9.75 ± 0.08	12.60 ± 1.10	12.92 ± 1.44^{i}
CAT (µmol/g tissue)	1.86 ± 0.11	1.93 ± 0.28	1.26 ± 0.01	2.52 ± 0.40	2.51 ± 0.32
GSH (µmol/g tissue)	1.87 ± 0.08	1.65 ± 0.02^{a}	1.27 ± 0.02^{c,k}	1.72 ± 0.06	1.70 ± 0.06
MDA (µmol/g tissue)	22.20 ± 4.10	49.45 ± 3.38^{c}	40.42 ± 0.01^{a}	25.81 ± 5.31^{j}	26.76 ± 4.79^{j}
Ca (mg/dL)	0.68 ± 0.06	0.90 ± 0.02^{a}	0.83 ± 0.08	0.62 ± 0.02^{k}	0.64 ± 0.03^{k}
Na (mmol/L)	157.90 ± 2.00	154.90 ± 2.25	159.70 ± 3.56	156.42 ± 6.99	154.00 ± 2.90
K (mmol/L)	3.87 ± 0.29	4.42 ± 0.14	5.16 ± 0.33	3.58 ± 0.65	3.82 ± 0.40
HCO_3 (mmol/L)	16.96 ± 1.05	21.35 ± 0.92^{b}	20.99 ± 0.87^{b}	17.02 ± 0.72^{k}	17.47 ± 0.31^{k}
BUN (mg/dL)	8.70 ± 0.27	9.06 ± 0.17	8.25 ± 0.32	8.43 ± 0.28	8.40 ± 0.32
CRE (mg/dL)	0.59 ± 0.08	1.24 ± 0.18^{b}	1.60 ± 0.37^{a}	0.65 ± 0.08^{j}	0.62 ± 0.05^{j}

SOD – superoxide dismutase, CAT – catalase, GSH - glutathione, MDA – malonaldehyde, Ca – Calcium, Na – Sodium, K – potassium, HCO_3 – Bicarbonate, BUN – blood urea nitrogen, CRE – Creatinine
^{a,b,c} significant in comparison to A. ^{i,j,k} significant in comparison to B
$^{a=i}$ p = 0.05, $^{b=j}$ p = 0.01, $^{c=k}$ p = 0.00.

Table 3b. Kidney biochemical levels of the untreated and the treated rats at 40 kV on day 30.

Indicators	A	B	C	D	E
SOD (µmol/g tissue)	22.77 ± 4.56	17.55 ± 2.70	16.19 ± 3.54	20.50 ± 4.70	20.63 ± 3.36
CAT (µmol/g tissue)	2.59 ± 0.59	1.70 ± 0.76	1.26 ± 0.23	2.13 ± 0.63	2.08 ± 0.68
GSH (µmol/g tissue)	1.45 ± 0.15	0.92 ± 0.05^{a}	0.87 ± 0.21^{a}	1.53 ± 0.08^{i}	1.63 ± 0.19^{j}
MDA (µmol/g tissue)	20.92 ± 4.40	66.71 ± 7.15^{c}	50.23 ± 9.60^{a}	25.01 ± 3.82^{j}	24.75 ± 6.88^{j}
Ca (mg/dL)	0.79 ± 0.10	0.67 ± 0.08	1.06 ± 0.15^{a}	0.82 ± 0.06	0.75 ± 0.15
Na (mmol/L)	103.30 ± 6.15	117.90 ± 12.57	99.11 ± 3.75	105.10 ± 7.10	104.30 ± 4.87
K (mmol/L)	3.00 ± 0.62	2.85 ± 0.03	6.62 ± 0.03^{c,k}	3.56 ± 0.37^{j}	3.69 ± 0.53^{j}
HCO_3 (mmol/L)	34.23 ± 3.11	35.19 ± 2.32	29.43 ± 2.32	35.09 ± 2.54	33.93 ± 1.06
BUN (mg/dL)	6.35 ± 0.58	8.69 ± 0.68^{b}	7.77 ± 0.07^{c}	6.52 ± 0.31^{j}	6.47 ± 0.09^{j}
CRE (mg/dL)	0.67 ± 0.06	1.24 ± 0.18^{b}	1.58 ± 0.11^{a}	0.65 ± 0.18^{i}	0.66 ± 0.35^{i}

Table 4a. Kidney biochemical levels of the untreated and the treated rats at 80 kV on day 1

Indicators	A	B	C	D	E
SOD (µmol/g tissue)	12.16 ± 0.83	9.17 ± 2.30	9.56 ± 0.20	12.70 ± 0.54	12.83 ± 3.10
CAT (µmol/g tissue)	1.86 ± 0.11	1.38 ± 0.03^{a}	1.11 ± 0.12^{c}	2.45 ± 0.02^{b,j}	2.43 ± 0.17^{b,j}
GSH (µmol/g tissue)	1.87 ± 0.08	0.99 ± 0.12^{c}	0.79 ± 0.01^{c}	1.72 ± 0.13^{k}	1.77 ± 0.02^{k}
MDA (µmol/g tissue)	22.20 ± 4.10	52.70 ± 2.99^{c}	53.15 ± 2.50^{c}	23.39 ± 1.53^{k}	25.94 ± 2.82^{k}
Ca (mg/dL)	0.68 ± 0.06	0.84 ± 0.03	0.97 ± 0.08^{c}	0.70 ± 0.02^{j}	0.69 ± 0.06^{j}
Na (mmol/L)	157.90 ± 2.00	154.60 ± 5.09	140.10 ± 1.65^{b,i}	140.60 ± 3.10^{b,i}	140.00 ± 1.99
K (mmol/L)	3.87 ± 0.29	3.88 ± 0.22	4.88 ± 0.23	3.53 ± 0.37	3.37 ± 0.45
HCO_3 (mmol/L)	16.96 ± 1.05	23.73 ± 0.50^{c}	22.15 ± 0.43^{c}	17.05 ± 0.77	16.21 ± 0.37^{i}
BUN (mg/dL)	8.70 ± 0.27	10.16 ± 0.41	9.80 ± 0.60	8.62 ± 1.66	8.74 ± 0.66
CRE (mg/dL)	0.59 ± 0.08	0.94 ± 0.06^{b}	1.23 ± 0.13^{a,i}	0.56 ± 0.34	0.62 ± 0.10

Table 4b. Kidney biochemical levels of the untreated and the treated rats at 80 kV on day 30

Indicators	A	B	C	D	E
SOD (µmol/g tissue)	22.77 ± 4.56	12.50 ± 1.04^{a}	13.24 ± 1.20	23.88 ± 1.71^{k}	22.21 ± 2.92^{j}
CAT (µmol/g tissue)	2.59 ± 0.59	1.85 ± 0.67	1.64 ± 0.65	2.66 ± 0.80	2.74 ± 0.87
GSH (µmol/g tissue)	1.45 ± 0.15	1.09 ± 0.19	1.15 ± 0.15	1.37 ± 0.15	1.42 ± 0.12
MDA (µmol/g tissue)	20.92 ± 4.40	50.17 ± 11.36^{a}	53.65 ± 10.72^{a}	21.01 ± 3.03	22.52 ± 3.56
Ca (mg/dL)	0.79 ± 0.10	0.62 ± 0.05	0.75 ± 0.08	0.78 ± 0.28	0.77 ± 0.12
Na (mmol/L)	103.30 ± 6.15	111.80 ± 7.31	104.30 ± 7.00	104.90 ± 3.21	105.00 ± 4.21
K (mmol/L)	3.00 ± 0.62	2.14 ± 0.58	5.01 ± 0.67^{a,j}	3.14 ± 0.29	3.21 ± 0.13
HCO_3 (mmol/L)	34.23 ± 3.11	40.96 ± 0.30	34.62 ± 7.01	34.32 ± 1.10	34.21 ± 1.60
BUN (mg/dL)	6.35 ± 0.58	6.94 ± 1.17	6.85 ± 0.38	6.32 ± 0.25	6.38 ± 0.38
CRE (mg/dL)	0.67 ± 0.06	1.50 ± 0.37^{a}	0.78 ± 0.18	0.69 ± 0.21^{j}	0.65 ± 0.12^{j}

Effects on renal biochemicals

The results obtained for the assay of renal biochemicals post-treatment at the diagnostic x-ray voltage are presented in Tables 3 to 5, respectively. At 40 kV (Table 3a and b), there was a decrease in the SOD, CAT, and GSH activity with an increase in the MDA activity of the rats in groups B and C compared to those of the baseline control (group A). This was, however, not so for those in groups D and E, as there was an increase in the SOD, CAT, and GSH activity with a slight increase in the MDA activity of the groups injected with the biosynthesized AuNPs. This translated to the differences observed in the level of the electrolytes Ca, Na, K and HCO_3, BUN, and CRE of the rats. As observed in the values obtained at 40 kV, the results of the biochemicals followed the same trend at 80 kV and 120 kV of x-ray tube voltage (Tables 4a - 5b).

Table 5a. Kidney biochemical level of the untreated and the treated rats at 120 kV on day 1

Indicators	A	B	C	D	E
SOD (µmol/g tissue)	12.16 ± 0.83	7.40 ± 0.44^{a}	6.36 ± 0.87^{b}	12.33 ± 1.52^{i}	12.55 ± 1.36^{i}
CAT (µmol/g tissue)	1.86 ± 0.11	0.56 ± 0.11^{c}	0.96 ± 0.10^{c}	1.71 ± 0.24^{k}	1.57 ± 0.09^{k}
GSH (µmol/g tissue)	1.87 ± 0.08	1.26 ± 0.06^{c}	1.09 ± 0.10^{c}	1.75 ± 0.06^{k}	1.75 ± 0.04^{k}
MDA (µmol/g tissue)	22.20 ± 4.10	47.46 ± 1.76^{c}	47.92 ± 3.37^{c}	30.82 ± 4.88^{j}	31.74 ± 2.94^{i}
Ca (mg/dL)	0.68 ± 0.06	0.93 ± 0.06^{a}	0.80 ± 0.11	0.71 ± 0.03	0.75 ± 0.05
Na (mmol/L)	157.90 ± 2.00	142.10 ± 1.26^{b}	135.80 ± 2.91^{c}	135.80 ± 5.28^{c}	136.00 ± 1.45^{b}
K (mmol/L)	3.87 ± 0.29	3.96 ± 0.13	4.42 ± 0.23	3.68 ± 0.43	3.82 ± 0.15
HCO_3 (mmol/L)	16.96 ± 1.05	20.92 ± 0.38^{a}	21.66 ± 0.26^{b}	17.01 ± 0.09^{k}	16.92 ± 0.16^{j}
BUN (mg/dL)	8.70 ± 0.27	10.49 ± 0.40	10.60 ± 0.79	10.65 ± 0.57	10.24 ± 0.84
CRE (mg/dL)	0.59 ± 0.08	0.92 ± 0.02	1.31 ± 0.10^{a}	0.63 ± 0.12	0.60 ± 0.21

Table 5b. Kidney biochemical levels of the untreated and the treated rats at 120 kV on day 30

Indicators	A	B	C	D	E
SOD (µmol/g tissue)	22.77 ± 4.56	14.01 ± 2.27	16.50 ± 2.05	23.88 ± 1.71	20.16 ± 0.83
CAT (µmol/g tissue)	2.59 ± 0.59	1.20 ± 0.36	1.29 ± 0.47	2.41 ± 1.23	2.45 ± 0.44
GSH (µmol/g tissue)	1.45 ± 0.15	0.69 ± 0.02^{k}	0.87 ± 0.17^{a}	1.36 ± 0.08^{k}	1.23 ± 0.11^{j}
MDA (µmol/g tissue)	20.92 ± 4.40	64.35 ± 7.30^{c}	55.98 ± 10.75^{b}	29.45 ± 4.96^{i}	29.68 ± 6.81^{i}
Ca (mg/dL)	0.79 ± 0.10	0.95 ± 0.05	1.39 ± 0.26	0.75 ± 0.17	0.76 ± 0.05
Na (mmol/L)	103.30 ± 6.15	106.20 ± 6.92	100.30 ± 8.46	102.30 ± 2.06	103.23 ± 3.26
K (mmol/L)	3.00 ± 0.62	3.12 ± 0.73	3.19 ± 0.77	2.98 ± 0.30	3.00 ± 0.21
HCO_3 (mmol/L)	34.23 ± 3.11	39.04 ± 2.05	33.46 ± 3.60	33.46 ± 0.94	34.23 ± 0.23
BUN (mg/dL)	6.35 ± 0.58	7.00 ± 1.20	8.77 ± 0.55	6.54 ± 0.06	6.75 ± 0.35
CRE (mg/dL)	0.67 ± 0.06	1.61 ± 0.34	1.50 ± 0.38	0.69 ± 0.16^{j}	0.71 ± 0.05^{j}

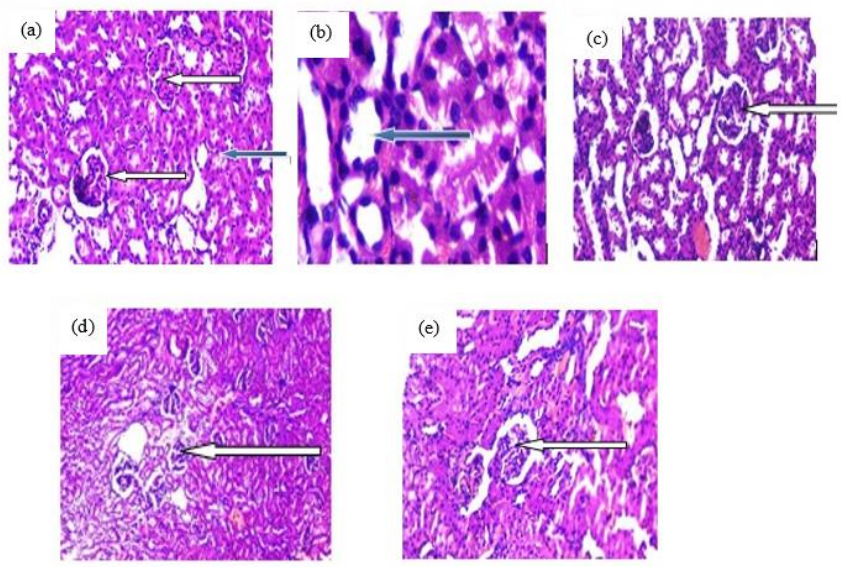

Figure 4. Photomicrograph of the kidney sections of the rats stained with H & E showing normal architecture as seen in lower magnification x100, the renal cortex shows normal glomeruli with normal mesangial cells and capsular spaces (white arrow), the renal tubules appear normal (blue arrow), the interstitial spaces appear normal (slender arrow).

Histopathological findings

Histopathological examination of the kidney tissue stained with H & E demonstrated normal architecture four weeks post-treatment, as revealed in Figure 4. The renal cortex appears normal, with normal glomeruli, mesangial cells, and capsular gaps for all the groups. Additionally, the renal tubules showed typical interstitial spaces. Therefore, no morphological abnormalities or obvious pathological lesions that could be linked to the administration of AuNPs to the rats were seen in the histological examinations of the sections for the rats injected with the biosynthesized AuNPs. This is in line with the kidney biochemical test results and the fact that the drugs were removed from circulation.

Discussion

Radiographic imaging utilizes tube voltages (kV) that vary from a low of 25 kV in mammography to a high of 140 kV in chest imaging. The choice of kV for a particular imaging task is influenced by the required contrast. For materials with low atomic numbers (Z), like soft tissue and bodily fluids, this adjustment is generally restricted to lower kV values. In contrast, the radiographic contrast produced by materials with higher atomic numbers, such as calcium, iodine, and barium, is affected by a broader range of kV values. As such, the ability of X-ray photons to pass through matter is determined by their energy levels. High-energy X-ray photons are more capable of penetrating substances, while lower-energy photons are more likely to be absorbed. Consequently, a higher kV and mean energy of the x-ray beam result in improved penetration through materials, which may not significantly enhance the radiographic contrast. This was evident by the radiographic image obtained at the x-ray tube voltage investigated for the rats that were not administered any of the substances (Figure 2). Thus, in Figure 3, the radiograph of the rats in groups D (administered with *P. guajava* capped AuNPs) and E (administered with *C. olitorius* capped AuNPs) is a confirmation that plant-based AuNPs enable clear contrast in comparison to those of groups B (without CA) and C (administered with iodine-based CA, Urografin). Thus, biosynthesized AuNPs can serve as an x-ray contrast agent and even perform better than the ICA due to the high atomic number of the binding element of gold (Z = 79) compared to that of iodine (Z = 53), high absorption coefficient (at 100 keV: gold = 5.16 cm^2 g^{-1}, iodine = 1.94 cm^2 g^{-1}; soft tissue: 0.169 cm^2 g^{-1}; and bone: 0.186 cm^2 g^{-1}), thus providing approximately three-fold absorption more than iodine [27]. The increase in the surface area of AuNPs also makes the solution penetrate and traverse several absorbing mediums than iodine. More so, imaging Au at 80 – 100 keV reduces interference from bone absorption and takes advantage of lower soft tissue absorption, which will reduce patient radiation dose. Studies also showed that even when concentrated, AuNP solutions were similar to water in viscosity, compared with the iodine-based contrast agent that needs high viscosity to obtain sharp radiographic contrast [27, 30].

The kidney is an essential organ that carries out critical functions, including the removal of both non-toxic and toxic substances generated during metabolic processes, the management of internal fluid balance, and the secretion of hormones that help evaluate kidney health. Antioxidant enzymes such as superoxide dismutase (SOD), catalase (CAT), and glutathione (GSH) play protective roles against reactive oxygen species (ROS). Lipid peroxidation significantly influences the production of free radicals, with malondialdehyde (MDA) serving as a prominent product and a key indicator of oxidative stress [22, 23, 50, 51]. Consequently, a reduction in SOD, CAT, and GSH levels, alongside an increase in MDA levels, leads to a rise in inactive ROS, which can hinder the functioning of renal cells [52]. As a result, the renal tissue experiences considerable stress. The data collected indicated a marked decrease in the activities of SOD, CAT, and GSH in the rats from groups B and C, along with an elevation in MDA levels for each diagnostic x-ray voltage tested, compared to the control group (group A). Conversely, rats in groups D and E exhibited a notable increase in SOD, CAT, and GSH activities, coupled with a reduction in MDA activity, relative to the baseline control (group A) and the experimental control (group B). This effect may be linked to the various phytochemicals found in the plants utilized (*P. guajava and C. olitorius*), further confirming the anti-inflammatory properties of these plants.

Electrolytes such as sodium (Na), potassium (K), and bicarbonate (HCO_3) are charged particles that facilitate the transmission of nerve and muscle signals throughout the body. Sodium and potassium serve as the main cations (positively charged ions), while bicarbonate is one of the key anions (negatively charged ions) present in the plasma. Calcium plays a vital role in various processes, including muscle contraction, activation of oocytes, formation of strong bones and teeth, blood clotting, transmission of nerve impulses, regulation of heartbeat, and maintaining fluid balance within cells. A malfunction in the kidneys can disrupt the balance of fluids and electrolytes, resulting in an imbalance of specific electrolytes. This, in turn, can interfere with the transmission of nerve and muscle impulses throughout the body, potentially leading to serious consequences for renal function. Moreover, when the kidneys fail, whether acutely or chronically, the byproducts of nitrogen metabolism accumulate, causing elevated levels of nonprotein nitrogen reflected in increased blood urea nitrogen (BUN) and serum creatinine (CRE) [53, 54]. Elevated levels of BUN and CRE may indicate that the kidneys are not functioning properly. Therefore, the measurements of electrolytes and biochemicals align with the findings from biomarkers of oxidative stress, showing that the rats in groups B and C are experiencing stress, while those in groups D and E are not.

Table 6. Comparison of the findings of the present study with some other studies.

Indicators	Hainfeld *et al.* [27]	Al-Neami *et al.* [30]	Lee *et al.* [58]	Present Study	
				P. guajava	*C. olitorius*
AuNPs size	1.90 ± 0.10	38.50	12.80	8.23 ± 1.03	6.57 ± 1.62
Preparation	Purchased	Citrate reduction method	Purchased	Biological method	
X-ray voltage	22	40	-	40	40
Animal used	Balb/C mice	Mice	Sprague-Dawley rats	Wistar rats	Wistar rats
SOD	-	-	-	20.50 ± 4.70	20.63 ± 3.36
CAT	-	-	-	2.13 ± 0.63	2.08 ± 0.68
GSH	-	-	-	1.53 ± 0.08	1.63 ± 0.19
MDA	-	-	-	25.01 ± 3.82	24.75 ± 6.88
Ca	10.70 ± 1.40	-	9.57 ± 0.12	0.82 ± 0.06	0.75 ± 0.15
Na	-	-	145.33 ± 0.67	105.10 ± 7.10	104.30 ± 4.87
K	-	-	4.47 ± 0.12	3.56 ± 0.37	3.69 ± 0.53
HCO_3	-	-	-	35.09 ± 2.54	33.93 ± 1.06
BUN	28.40 ± 4.30	-	14.37 ± 1.21	6.52 ± 0.31	6.47 ± 0.09
CRE	0.00 ± 0.10	-	0.48 ± 0.0.04	0.65 ± 0.18	0.66 ± 0.35

All indicators remain as earlier defined; the negative sign (–) indicates data is not available or analysis is not carried out
AuNPs size (nm), X-ray voltage (kV), SOD (µmol/g tissue), CAT (µmol/g tissue), GSH (µmol/g tissue), MDA (µmol/g tissue), Ca (mmol/L), Na (mmol/L), K (mmol/L), HCO_3 (mmol/L), BUN (mg/dL), CRE (mg/dL)

Hence, with the findings obtained for the assay of the biochemical indicators, a trace of acute kidney injury (AKI) was observed both on day 1- and four-week post-treatment in the rats of groups B (without CA, x-ray only) and C (administered with iodine-based CA, Urografin). An action that may lead to a decrease in kidney functions due to a reduction in the performance of nephrons, thus resulting in the kidney not functioning properly, and also leads to contrast-induced nephrotoxicity (CIN), which is one of the limitations of the existing iodinated CA. However, those injected with the AuNPs from groups D and E did not exhibit any form of kidney injury, as the organs were protected by the antioxidants present in the leaves of the plants used for the synthesis of the AuNPs. The results obtained for all other indicators of kidney injury for the rats of groups D and E showed that plant-based AuNPs, when used as CA, pose no threat to renal function, unlike the iodinated CA.

The radiograph results support the use of AuNPs as x-ray imaging contrast agents, as suggested by various reports [27–30]. In particular, biologically synthesized AuNPs are more economical, easily reproducible, and environmentally friendly than other AuNP synthesis methods. Hence, the application of biosynthesized AuNPs will open new fields of medical imaging for other x-ray imaging modalities such as mammography, computed tomography, renal angiography, and many more, as this will enable non-invasive detection of tumors that are hidden with fat and unintentionally missed during imaging examinations. The utilization of a small quantity of AuNPs as a contrast agent in imaging will also improve the safety margin in radiological examinations and thus ensure the as low as reasonably achievable (ALARA) policy of the International Commission of Radiological Protection (ICRP).

The values obtained for the assessment of kidney injury in this present study fall below the findings of Hainfeld *et al.*, reporting the administration of 1.9 ± 0.1 nm AuNPs to mice and exposing them to 22 kV and eight mAs of x-ray from a mammography unit [27]. The range of values obtained also conformed with the values obtained in other studies reporting the diverse biomedical applications of AuNPs (Table 6) [55-60].

Conclusion

The findings of the study demonstrated that biosynthesized gold nanoparticles (AuNPs) can serve as x-ray contrast agents (CAs) as the AuNPs enable radiographic contrast and also protect against nephropathy compared to the iodine-based CAs. This is due to a number of factors, including the fact that gold has a higher atomic number than iodine, attenuation properties, a larger surface area, biocompatibility, anti-inflammatory qualities, and the availability of plants that are used as reducing agents in the production of gold nanoparticles. These factors can all be used to create a variety of biomedical applications. This work, therefore, supports previous research that suggests using AuNPs as x-ray CA, with a focus on biosynthesized AuNPs.

Acknowledgements

The authors would like to thank the technical staff and radiographer at the Ladoke Akintola University of Technology Health Center's Radiography Unit for helping to make the research a reality.

References

1. Bae KT. Intravenous contrast medium administration and scan timing at CT: considerations and approaches. Radiology. 2010 Jul;256(1):32-61.
2. Ayanlola PS, Isola GA, Saka WA, Akinloye MK, Sanusi YK, Adedokun O, et al. Cardioprotective role of biosynthesized gold nanoparticles compared to an iodinated-based x-ray contrast agent in Male Wistar

Rats. Nanomedicine Research Journal. 2023 Mar 1;8(1):24-36.
3. Bushberg JT, Boone JM. The essential physics of medical imaging. Lippincott Williams & Wilkins; 2011 Dec 20.
4. Suetens P. Fundamentals of medical imaging. Cambridge university press; 2017 May 11.
5. Nash K, Hafeez A, Hou S. Hospital-acquired renal insufficiency. American Journal of Kidney Diseases. 2002 May 1;39(5):930-6.
6. Stacul F, Van der Molen AJ, Reimer P, Webb JA, Thomsen HS, Morcos SK, et al. Contrast induced nephropathy: updated ESUR contrast media safety committee guidelines. European radiology. 2011 Dec;21:2527-41.
7. Faucon AL, Bobrie G, Clément O. Nephrotoxicity of iodinated contrast media: From pathophysiology to prevention strategies. European Journal of Radiology. 2019 Jul 1;116:231-41.
8. Ludwig U, Keller F. Prophylaxis of contrast-induced nephrotoxicity. BioMed research international. 2014;2014(1):308316.
9. Bhatt S, Rajpal N, Rathi V, Avasthi R. Contrast induced nephropathy with intravenous iodinated contrast media in routine diagnostic imaging: an initial experience in a tertiary care hospital. Radiology research and practice. 2016;2016(1):8792984.
10. Shams E, Mayrovitz HN. Contrast-induced nephropathy: a review of mechanisms and risks. Cureus. 2021 May;13(5).
11. Dröge W. Free radicals in the physiological control of cell function. Physiological reviews. 2002.
12. Genestra M. Oxyl radicals, redox-sensitive signalling cascades and antioxidants. Cellular signalling. 2007 Sep 1;19(9):1807-19.
13. Valko M, Leibfritz D, Moncol J, Cronin MT, Mazur M, Telser J. Free radicals and antioxidants in normal physiological functions and human disease. The international journal of biochemistry & cell biology. 2007 Jan 1;39(1):44-84.
14. Rajendran P, Nandakumar N, Rengarajan T, Palaniswami R, Gnanadhas EN, Lakshminarasaiah U, et al. Antioxidants and human diseases. Clinica chimica acta. 2014 Sep 25;436:332-47.
15. Pizzino G, Irrera N, Cucinotta M, Pallio G, Mannino F, Arcoraci V, et al. Oxidative stress: harms and benefits for human health. Oxidative medicine and cellular longevity. 2017;2017(1):8416763.
16. Halliwell B. Antioxidants in human health and disease. Annual review of nutrition. 1996 Jul;16(1):33-50.
17. Devasagayam TP, Tilak JC, Boloor KK, Sane KS, Ghaskadbi SS, Lele RD. Free radicals and antioxidants in human health: current status and future prospects. Japi. 2004 Oct 25;52(794804):4.
18. Lobo V, Patil A, Phatak A, Chandra N. Free radicals, antioxidants and functional foods: Impact on human health. Pharmacognosy reviews. 2010 Jul;4(8):118.
19. Finkel T. Signal transduction by reactive oxygen species. Journal of Cell Biology. 2011 Jul 11;194(1):7-15.
20. Ray PD, Huang BW, Tsuji Y. Reactive oxygen species (ROS) homeostasis and redox regulation in cellular signaling. Cellular signalling. 2012 May 1;24(5):981-90.
21. Phaniendra A, Jestadi DB, Periyasamy L. Free radicals: properties, sources, targets, and their implication in various diseases. Indian journal of clinical biochemistry. 2015 Jan;30:11-26.
22. Katerji M, Filippova M, Duerksen-Hughes P. Approaches and methods to measure oxidative stress in clinical samples: Research applications in the cancer field. Oxidative medicine and cellular longevity. 2019;2019(1):1279250.
23. Dasgupta A, Wahed A. Clinical chemistry, immunology and laboratory quality control: a comprehensive review for board preparation, certification and clinical practice.
24. Liss P, Nygren A, Erikson U, Ulfendahl HR. Injection of low and iso-osmolar contrast medium decreases oxygen tension in the renal medulla. Kidney international. 1998 Mar 1;53(3):698-702.
25. Rosenberger C, Rosen S, Heyman SN. Renal parenchymal oxygenation and hypoxia adaptation in acute kidney injury. Clinical and experimental pharmacology & physiology. 2006 Oct 1;33(10):980-8.
26. Pisani A, Riccio E, Andreucci M, Faga T, Ashour M, Di Nuzzi A, et al. Role of reactive oxygen species in pathogenesis of radiocontrast-induced nephropathy. BioMed research international. 2013;2013(1):868321.
27. Hainfeld JF, Slatkin DN, Focella TM, Smilowitz HM. Gold nanoparticles: a new X-ray contrast agent. The British journal of radiology. 2006 Mar 1;79(939):248-53.
28. Cormode DP, Skajaa T, Fayad ZA, Mulder WJ. Nanotechnology in medical imaging: probe design and applications. Arteriosclerosis, thrombosis, and vascular biology. 2009 Jul 1;29(7):992-1000.
29. De La Vega JC, Häfeli UO. Utilization of nanoparticles as X-ray contrast agents for diagnostic imaging applications. Contrast media & molecular imaging. 2015 Mar;10(2):81-95.
30. Al-Neami AQ, Al-Karam LQ, Humadi MD, Alwan MH. Applications and advantages of gold nanoparticles as X-ray contrast agent. J Biomed Eng Med Devic. 2017;2(2):1-3.
31. Gharatape A, Salehi R. Recent progress in theranostic applications of hybrid gold nanoparticles. European journal of medicinal chemistry. 2017 Sep 29;138:221-33.
32. Guo J, Rahme K, He Y, Li LL, Holmes JD, O′ Driscoll CM. Gold nanoparticles enlighten the future of cancer theranostics. International journal of nanomedicine. 2017 Aug 22:6131-52.
33. Seltzer SE, Blau M, Herman LW, Hooshmand RL, Herman LA, Adams DF, et al. Contrast material-carrying liposomes: biodistribution, clearance, and imaging characteristics. Radiology. 1995 Mar;194(3):775-81.
34. Isola GA, Akinloye MK, Sanusi YK, Ayanlola PS, Alamu GA. Optimizing X-Ray Imaging Using Plant Mediated Gold Nanoparticles as Contrast Agent: A Review. International Journal of Research and Scientific Innovation. 2021;8(8):169-75.
35. Jadoun S, Arif R, Jangid NK, Meena RK. Green synthesis of nanoparticles using plant extracts: A review. Environmental Chemistry Letters. 2021 Feb;19(1):355-74.
36. Sultana S, Djaker N, Boca-Farcau S, Salerno M, Charnaux N, Astilean S, et al. Comparative toxicity

evaluation of flower-shaped and spherical gold nanoparticles on human endothelial cells. Nanotechnology. 2015 Jan 9;26(5):055101.
37. Bhamidipati M, Fabris L. Multiparametric assessment of gold nanoparticle cytotoxicity in cancerous and healthy cells: the role of size, shape, and surface chemistry. Bioconjugate chemistry. 2017 Feb 15;28(2):449-60.
38. Pujalté I, Passagne I, Brouillaud B, Tréguer M, Durand E, Ohayon-Courtès C, et al. Cytotoxicity and oxidative stress induced by different metallic nanoparticles on human kidney cells. Particle and fibre toxicology. 2011 Dec;8:1-6.
39. Kermanizadeh A, Vranic S, Boland S, Moreau K, Baeza-Squiban A, Gaiser BK, et al. An in vitro assessment of panel of engineered nanomaterials using a human renal cell line: cytotoxicity, pro-inflammatory response, oxidative stress and genotoxicity. BMC nephrology. 2013 Dec;14:1-2.
40. Jha AK, Prasad K, Prasad K, Kulkarni AR. Plant system: nature's nanofactory. Colloids and Surfaces B: Biointerfaces. 2009 Oct 15;73(2):219-23.
41. Thakkar KN, Mhatre SS, Parikh RY. Biological synthesis of metallic nanoparticles. Nanomedicine: nanotechnology, biology and medicine. 2010 Apr 1;6(2):257-62.
42. Yasmin A, Ramesh K, Rajeshkumar S. Optimization and stabilization of gold nanoparticles by using herbal plant extract with microwave heating. Nano convergence. 2014 Apr 11;1(1):12.
43. Kumar M, Tomar M, Amarowicz R, Saurabh V, Nair MS, Maheshwari C, et al. Guava (Psidium guajava L.) leaves: Nutritional composition, phytochemical profile, and health-promoting bioactivities. Foods. 2021 Apr 1;10(4):752.
44. Ismail EH, Saqer AM, Assirey E, Naqvi A, Okasha RM. Successful green synthesis of gold nanoparticles using a Corchorus olitorius extract and their antiproliferative effect in cancer cells. International journal of molecular sciences. 2018 Sep 3;19(9):2612.
45. Yokoyama S, Hiramoto K, Fujikawa T, Kondo H, Konishi N, Sudo S, et al. Topical application of Corchorus olitorius leaf extract ameliorates atopic dermatitis in NC/Nga mice. Dermatol Aspects. 2014;2(3):10-7243.
46. National Research Council. Guide for the Care and Use of Laboratory Animals Eighth Edition. Washington, DC: The National Academies Press. 2011
47. Turner PV, Brabb T, Pekow C, Vasbinder MA. Administration of substances to laboratory animals: routes of administration and factors to consider. Journal of the American Association for Laboratory Animal Science. 2011 Sep 15;50(5):600-13.
48. Abdelhalim MA, Moussa SA. The gold nanoparticle size and exposure duration effect on the liver and kidney function of rats: In vivo. Saudi journal of biological sciences. 2013 Apr 1;20(2):177-81.
49. Pandy V. A simple method for animal dose calculation in preclinical research. EC Pharmacol Toxicol. 2020;8:1-2.
50. Halliwell B, Gutteridge JC. Lipid peroxidation, oxygen radicals, cell damage, and antioxidant therapy. The Lancet. 1984 Jun 23;323(8391):1396-7.
51. Chaudière J, Ferrari-Iliou R. Intracellular antioxidants: from chemical to biochemical mechanisms. Food and chemical toxicology. 1999 Sep 1;37(9-10):949-62.
52. Forsyth P, Fleming L, Moir L, Mcclusky L, Watson N, Meiklejohn J, et al. Improving medication adherence in patients with chronic heart failure: a feasibility study.
53. Fedorova S, Miyamoto R, Harada T, Isogai S, Hashimoto H, Ozato K, et al. Renal glomerulogenesis in medaka fish, Oryzias latipes. Developmental Dynamics: An Official Publication of the American Association of Anatomists. 2008 Sep;237(9):2342-52.
54. Kaid F, Alabsi AM, Alafifi N, Ali-Saeed R, Ameen Al-koshab M, Ramanathan A, et al. Histological, biochemical, and hematological effects of goniothalamin on selective internal organs of male sprague-dawley rats. Journal of Toxicology. 2019;2019(1):6493286.
55. Zhang Z, Ross RD, Roeder RK. Preparation of functionalized gold nanoparticles as a targeted X-ray contrast agent for damaged bone tissue. Nanoscale. 2010;2(4):582-6.
56. Bashandy MM, Ahmed AR, El-Gaffary M, Abd El-Rahman SS. Gold nanoparticle: synthesis, characterization, clinico-pathological, pathological, and bio-distribution studies in rabbits. International Journal of Pharmacological and Pharmaceutical Sciences. 2015 Nov 1;9(11):1168-74.
57. He Z, Li C, Zhang X, Zhong R, Wang H, Liu J, et al. The effects of gold nanoparticles on the human blood functions. Artificial cells, nanomedicine, and biotechnology. 2018 Nov 5;46(sup2):720-6.
58. Lee JH, Gulumian M, Faustman EM, Workman T, Jeon K, Yu IJ. Blood biochemical and hematological study after subacute intravenous injection of gold and silver nanoparticles and coadministered gold and silver nanoparticles of similar sizes. BioMed research international. 2018;2018(1):8460910.
59. Isoda K, Tanaka A, Fuzimori C, Echigoya M, Taira Y, Taira I, et al. Toxicity of gold nanoparticles in mice due to nanoparticle/drug interaction induces acute kidney damage. Nanoscale research letters. 2020;15:1-8.
60. Aljohani FS, Hamed MT, Bakr BA, Shahin YH, Abu-Serie MM, Awaad AK, et al. In vivo bio-distribution and acute toxicity evaluation of greenly synthesized ultra-small gold nanoparticles with different biological activities. Scientific reports. 2022 Apr 15;12(1):6269.